IEEE Access
Multidisciplinary | Rapid Review | Open Access Journal

Received June 12, 2019, accepted June 26, 2019, date of publication July 3, 2019, date of current version July 23, 2019.

Digital Object Identifier 10.1109/ACCESS.2019.2926542

Stereo Vision-Based Gamma-Ray Imaging for 3D Scene Data Fusion

PATHUM RATHNAYAKA[1], SEUNG-HAE BAEK[1], AND SOON-YONG PARK[2]
[1]School of Computer Science and Engineering, Kyungpook National University, Daegu 702-701, South Korea
[2]School of Electronics Engineering, College of IT Engineering, Kyungpook National University, Daegu 702-701, South Korea

Corresponding author: Soon-Yong Park (sypark@knu.ac.kr)

This work was supported in part by the National Research Foundation of Korea (NRF) funded by the Korea Government (MSIT: Ministry of Science and ICT) under Grant 2018M2A8A5083266, and in part by the BK21 Plus project funded by the Ministry of Education, South Korea, under Grant 21A20131600011.

ABSTRACT Modern developments of gamma-ray imagers by integrating multi-contextual sensors and advanced computer vision theories have enabled unprecedented capabilities in detection and imaging, reconstruction and mapping of radioactive sources. Notwithstanding these remarkable capabilities, the addition of multiple sensors such as light detection and ranging units (LiDAR), RGB-D sensors (Microsoft Kinect), and inertial measurement units (IMU) are mostly expensive. Instead of using such expensive sensors, we, in this paper, introduce a modest three-dimensional (3D) gamma-ray imaging method by exploiting the advancements in modern stereo vision technologies. A stereo line equation model is proposed to properly identify the distribution area of gamma-ray intensities that are used for two-dimensional (2D) visualizations. Scene data information of the surrounding environment captured at different locations are reconstructed by re-projecting disparity images created with the semi-global matching algorithm (SGM) and are merged together by employing the point-to-point iterative closest point algorithm (ICP). Instead of superimposing/overlaying 2D radioisotopes on the merged scene area, reconstructions of 2D gamma images are fused together with it to create a detailed 3D volume. Through experimental results, we try to emphasize the accuracy of our proposed fusion method.

INDEX TERMS Stereo vision, gamma-ray imaging, stereo matching, scene data fusion, 3D imaging.

I. INTRODUCTION

Detecting and imaging, localizing and volumetric-visualizing; gamma-ray sources are of the actively discussed topics in the field of radiology, since the discovery of X-rays in late 1895 [1]. Applications ranging from nuclear medicine to nuclear safeguards, nuclear contamination remediation, and even environmental monitoring are being widely researched [2]–[6], broadening the study of new designs and developments of much sophisticated gamma-ray imagers (detectors). Starting from medieval Geiger counters to modern static or portable imaging detectors with collimator, Compton, coded-aperture based approaches have been proposed in detecting and imaging [3].

The biggest challenge of most of these imagers is the correct differentiation between relevant and irrelevant information used to identify source intensities with scene data information and precise recognition of their spatial distributions. Though the use of Geiger counters had gradually increased; mainly after the incident in Fukushima, but they resulted in many wrong claims of radiation contamination. Also, they lack the ability to discriminate background radiation from the radioactivity [1].

As of other conventional means of gamma-ray imaging, collimators capable of determining incident angle - also known as line-of-response were used; especially in low energy nuclear medicine mainly after the development of the Anger camera [7]. However, these imagers showed significantly reduced efficiency at higher energy levels due to limited attenuation of gamma-rays in the collimator. Imagers with coded-apertures demonstrated some increased efficiency, however, limited to simple source configurations and low field of views [1].

On the other hand, Compton imaging and Compton scattering have been adopted into gamma-ray imaging, enabling source energy estimations and radioisotope identifications,

The associate editor coordinating the review of this manuscript and approving it for publication was Wen Chen.

source imaging and incidence direction reconstructions, and 3D position information measuring [8], [9]. Though these have received the most developments and are best suited for field use [12], they have certain downfalls. They require position sensitive detectors (PSDs) for high precision location estimations, the imaging capability is much confined at low energy levels, and the conic-type reconstructions sometimes wrap out-of-field sources to ghost locations on the back of the visualizations [12], [13].

A gamma-ray whose energy is measured is worth more than just the registration of its existence [1]. Notwithstanding coded aperture-based, collimator-based, and Compton scattering-based imaging approaches have been highly discussed in active radiation detection, they have shown very selective and/or less comprehensive visualization capabilities. In order to derive a better trade-off in gamma-ray imaging and visualizing, integration of many conceptual sensors has been proposed; providing new means in identifying matching distributions of gamma-ray sources with physical objects [10]. This lays the foundation of a new pathway for bringing the naked human eye a one-step closer to seeing and identifying spatial source distributions with more details in 3D world. The motivation of this research paper is to propose a stereo gamma detection camera equipped with a simple, and comparatively less expensive sensor fusion system for detailed gamma-ray visualization by deploying modern stereo computer vision theories. Unlike most contemporary sensor fusion systems been proposed, we do not use highly expensive contextual sensors, such as LiDAR or Kinects. As of our core work, we introduce a line equation model to properly localize gamma sources and a modest reconstruction method for their 3D scene data visualization.

The structure of our paper is as follows: Section *II* briefly discuss about a few contemporary state-of-the-art imaging systems with their scene data fusion methods. The design of our imager is roughly described in Section *III*, where a full description is given in our previous work [17]. 2D imaging of gamma-rays is challenging as they do not deposit their full energy in the detector, causing partial source imaging. On the other hand, pan/tilt-type imagers always have axis misalignment problems; leading into improper visualizations. We propose a stereo line-equation model to properly localize gamma sources, while compensating with partial imaging and misalignment problems. These localized intensities are then mapped into the 2D image coordinate to generate 2D gamma-ray images. This is briefly described in Section *IV*. Scene contexts of the surrounding environment captured at different locations from a CCD camera are reconstructed by re-projecting pixel points of disparity images generated based on Semi-Global Matching algorithm [19], [20]. Separate reconstructions of the scene context are merged together into a more detailed 3D volume by deploying the ICP algorithm [21], [22]. Similarly, 2D images of gamma-rays are reconstructed, merged, and fused with the merged scene reconstruction (Section *V*). Section *VI* summarizes our experimental results. As an additional measurement of determining source location, we calculate 3D distances from the imager to the center of the gamma source (Section $VI-A$). Inside our laboratory, we have used bright white-LED point sources as our radioactive materials, as they are broadly used in many radioactive researches [23]–[25]. Experiments using a Cs-137 source are done in a more secured radioactive facility. Both quantitative and qualitative result analyses (distance calculations and reconstructions) conducted to evaluate the accuracy of our proposed methods are also summarized. Finally, we conclude the paper by stating our thoughts and future improvements in Section *VII*.

II. CONTEMPORARY IMAGING SYSTEMS AND SCENE DATA FUSION

A series of scene data fusion techniques with many contextual sensor integration systems have been proposed throughout the past few years. Mihailescu et al. proposed the idea of combining a LiDAR sensor with their large field-of-view Compton imager to create 3D maps of the surrounding scene environment [8]. Though this approach instantiates the importance of volumetric visualizing, however, falls behind as only 2D spatial distributions of gamma sources are back-projected on the reconstruction area; causing localizing ambiguities (particularly when source distributions are fully/partially covered by obstacles). As an extension to this work, [11] discusses a full volumetric visualization and fusion approach of source distributions with scene data information, but yet fails in quality as volumetric models are created by hand using point cloud data of the LiDAR sensor [3].

As of other additional works, a series of more advanced imaging systems with sophisticated scene data fusion techniques have been proposed. Some enabled new means in registering and processing contextual information in real-time [10]. Barnowski *et al.* [3] discuss a near real-time gamma-ray imaging approach using Simultaneous Localization and Mapping (SLAM) for volumetric reconstructions of unknown environments. The cart-based Compton gamma-ray imager they used is designed by two 3D position-sensitive high purity germanium (HPGe) detectors. The 3D map of the surrounding environment is created by solving RGBD-SLAM, where RGB images and depth data are captured by a Microsoft Kinect sensor. The approach is suitable for indoor environments, however, not at outdoors as the IR camera of the Kinect sensor does not work properly in direct sunlight [14]. In addition, the reconstruction and tracking of gamma-ray events are not optimized for sensitivity, resulting in limited position resolution and Compton imaging efficiency.

An extended version of this approach is discussed in [1]. Two different gamma-ray imagers are presented - a second generation Compact Compton Imager (CCI-2) and a High-Efficiency Multimode Imager (HEMI). Like its predecessor, CCI-2 imager has a similar design, but equipped with additional contextual sensors: two panoramic video cameras and a LiDAR sensor for both indoor and outdoor data acquisition. They managed to solve the outdoor data acquisition

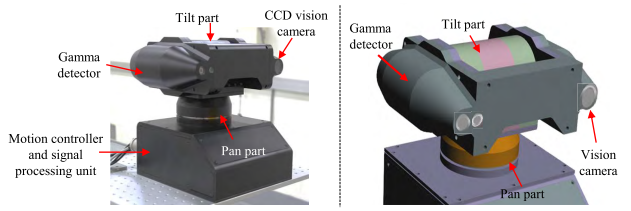

FIGURE 1. The design of our gamma-ray imager. Upper part consists of a gamma detector, vision camera, and a tilting module. The lower part contains a signal processing unit. Upper part is connected to the lower part through a panning module.

problem of their first generation imager by replacing the Kinect with a LiDAR sensor, however, this multi-sensor integration is more expensive.

The HEMI imager, consisting of 96 CdZnTe (CZT) crystals implemented in an active mask-type coplanar grid configuration, is used as a hand portable gamma-ray detector. The imager is sensitive to both low energy and high energy radiation, and the active mask configuration allows it to serve as a coded aperture and a Compton-type imager, simultaneously. This unit is upgraded in [15] by integrating a Kinect sensor, however, is susceptible to interference and, constrained by ambient lighting at outdoor environments [28].

The same unit is again used in [14] where various utilization and implementations are discussed. The Kinect sensor is used for indoor environments and RGBD-SLAM is employed for localizing and volumetric mapping. A video camera is used to replace the Kinect sensor for outdoor environments. In addition to hand-held deployment, the imager is mounted on an unmanned RMAX helicopter for aerial measurements. Scene data imagery is reconstructed using Structure-from-Motion [18] by finding SIFT features [16] in consecutive frames. Implementations discussed in this paper demonstrated significant improvements in the effective and accurate detection and mapping of gamma-ray sources, however, SIFT features require much power and heavy computational capabilities. Also, complexities in the environment (illumination variations) could lead to erroneous correspondence estimations, degrading reconstruction quality.

III. DESIGN OF THE GAMMA-RAY IMAGER

We designed a simple pan-tilt type gamma-ray imager as our development platform and is shown in Fig. 1. This is an upgraded version of our first generation gamma-ray imager described in [17]. The unit is a combination of a pinhole-type detector, tilting module, Point Grey CCD vision camera, panning module, and a signal-acquisition-and-processing unit (the term ''gamma-ray imager'' refers to the full complete device in Fig. 1, and ''detector'' to the assembly shown in Fig. 2). The detector is composed of a NaI(Tl) scintillator hybridized with a Hamamatsu H10722 small photo-multiplier tube (sPMT), a 10 mm diameter pinhole-type Lead (Pb) collimator, and a Tungsten (W) radiation shield case (Fig. 2). The surrounding shield is used to limit the radiation that reaches inside the pinhole. The vision camera is arranged to be horizontally linear with

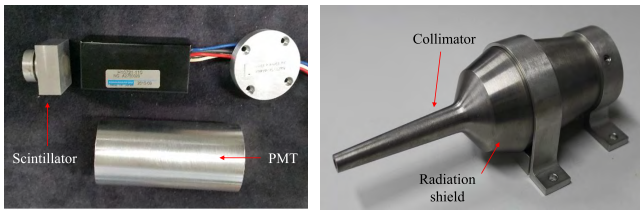

FIGURE 2. The design of gamma-ray detector: (a) internal structure, (b) outer structure of complete detector.

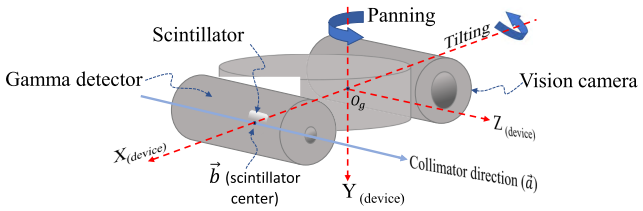

FIGURE 3. CAD model of the device in an ideal situation. The gamma detector lies on the right side and the vision camera on the left side.

the detector, connected to the tilting module that controls the vertical 360° rotation. The panning module connects detector+camera unit to the signal processing unit while controlling 360° horizontal rotation.

The only conceptual sensor we used with the gamma detector is the vision camera. The biggest challenge we had while designing the imager was how to obtain nearly-similar reconstruction capabilities as of state-of-the-art methods. The independent rotation of the imager in horizontal and vertical directions gave it a more standard stereo-type motion behavior, allowing the detector+camera assembly to interchange their positions with another. We placed high accurate brushless DC motors inside panning-tilting modules to ensure accurate symmetric rotations to the best of our knowledge. The way of capturing stereo data while rotating the imager is briefly described in our previous research work [17]. The weight of the full unit is about 16kg and mounted on top of a pedestal dolly providing support while moving around the environment to capture images at multiple locations.

IV. 2D GAMMA-RAY IMAGING: STEREO LINE EQUATION MODEL

In general, most pinhole-type mono gamma detectors follow a common 2D gamma-ray imaging approach. In a typical pan-tilt type detector, the contamination area is discretely scanned to localize gamma-rays passing through the opening of the collimator - known as the pinhole. These rays are sent into interaction with the scintillator and are converted into light photons detectable by the photomultiplier tube (PMT). These photons are converted into electronic signals with pulses and are recorded and mapped into pixel grey values of a 2D image. The accuracy of this process mostly depends on pan-tilt step interval, collimator length and diameter, and sensitivity of the scintillator. The opening of the collimator limits the field-of-view of the detector to a single pixel [12], controlling the resolution of the image in 2D view.

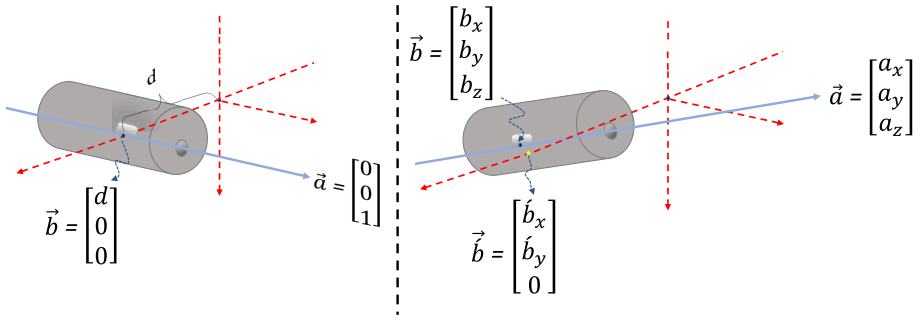

FIGURE 4. Side-by-side comparison between ideal and real situations. The symmetry is retained in the ideal situation (left), however, is not fulfilled in the real situation (right).

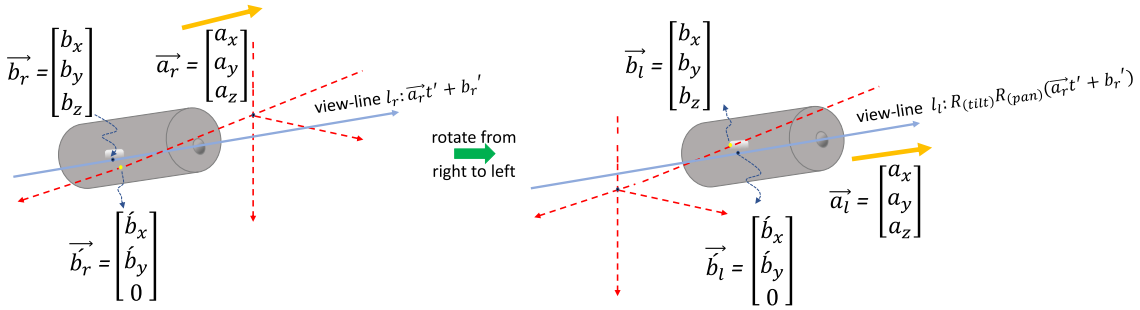

FIGURE 5. Rotating the device by 180° horizontally and vertically to change its position from right side to the left. Symmetry in the ideal situation is not maintained, however, compensated by employing the proposed line equation model. Only the gamma detector is shown for simple representation.

The initial state of the upper part of our gamma imager is shown as a CAD model in Fig. 3. We call this state as an ideal situation. Supposing the center-of-mass of the device (O_g) resembles the world coordinate system, the X-axis (X_{device}) passes through the center of the scintillator and is perpendicular to the Y-axis (Y_{device}). We can represent the direction vector of the collimator as a line (we call it as view-line l), which is in parallel with Z-axis (Z_{device}). Theoretically, we can assume that gamma-ray projections from 3D space lie along this view-line and the projected location can be shown mathematically as in (1):

$$l : \vec{a}t + \vec{b}, \tag{1}$$

where $\vec{a}$ and $\vec{b}$ represent the direction vector of the collimator and the center of the scintillator, respectively.

However, in real situations, it is difficult to proclaim that the symmetric alignment we see in the ideal situation is maintained. Aligning the scintillator center as perfect as in ideal situation is constrained due to irregular rotations of the motors used in panning and tilting modules. When rotating the detector horizontally and vertically to change its position from one side to the other (refer [17] to see how this rotation is done), guaranteeing it would come to its designated symmetric position is difficult. The detector can sometimes reside in bit slanted positions, creating an angle between scintillator center and the X_{device}. Fig. 4 depicts how sensors are aligned in an ideal situation and misaligned in a real situation, side-by-side (only the gamma detector is shown to minimize visual difficulties).

In such real situations, we cannot use (1) directly to localize 3D projections of gamma-rays. Instead of trying to calculate the mutual rotation and translation of the gamma detector with respect to world coordinate system, we try to solve this misalignment problem mathematically by modifying (1). Taking $\vec{b'}$ as the new intercepting point between the X_{device} and the scnitillator, we can summarize this attempt as in (2).

$$l' : \vec{a}(t + b_z/a_z) + \vec{b'} \equiv \vec{a}t' + \vec{b'} \tag{2}$$

Through out this whole paper, we lay our main interest on remedying the misalignment problem of the gamma detector more than the vision camera. This is done for the purpose of precise localization of gamma-rays passing through the collimator. We applied (2) immediately after moving it from either right side to left or left side to right. Fig. 5 shows such an instance where the gamma detector is rotated by 180° in both horizontal and vertical directions to move it from the right side to the left (only the movement of the gamma detector is shown as we mainly concentrate on rectifying its misalignment problem). If we take l_r represents the view-line of the collimator when the detector is at right side, we can use (2) to summarize this view-line as:

$$l_r : \vec{a_r}t' + \vec{b_r}' \tag{3}$$

Since we rotate the detector by known values in horizontal and vertical directions ($R_{(tilt)}$ and $R_{(pan)}$), we multiply them

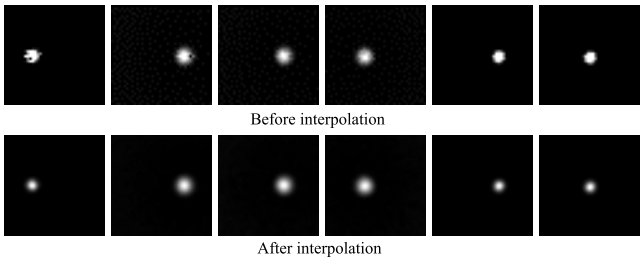

FIGURE 6. 2D imaging results of a Cs-137 gamma source before and after interpolation.

with scintillator center and right view-line, to represent the left view-line while compensating with the detector misalignment problem. This new relationship of the detector when it is moved into left side is mathematically shown in (4).

$$l_l : R_{(tilt)}R_{(pan)}(\vec{a}_r t' + \vec{b}'_r) \tag{4}$$

This novel line equation approach gave us the ability to Localize almost the full energy of sources while managing to solve partial 2D imaging problem discussed in previous sections.

After properly localizing rays and converting them into detectable signals, we can map them into the 2D coordinate system to create a detailed 2D image. However, this mapping is more discrete, giving a scattered representation (top tier in Fig. 6). As of post-processing, we applied an enhanced bilinear interpolation [26] to smooth discrete mappings. Some 2D imaging examples of a Cs-137 gamma source are shown in Fig. 6. The top tier depicts direct 2D imaging results of the source before interpolation and the bottom tier depicts respective interpolated results. It is visible that scattered/discrete representations of sources are properly processed.

V. STEREO MATCHING FOR 3D GAMMA-RAY AND SCENE RECONSTRUCTIONS

The motivation of 3D visualization of gamma-rays is to bring the naked human eye a one-step closer to seeing and identifying their contamination within the surrounding environment [10]. Previously described state-of-the-art methods use multi-sensors to capture contextual scene/environment data and exploit real-time mapping theories to fuse their reconstructions with spatial distributions of radioisotopes. However, in this research work, we try to arrive at this visualization by seeing it from a different perspective.

Our proposed visualization approach consists of four important steps: stereo image acquisition (both gamma-ray and scene data images), disparity image creation and reconstruction, ICP-based registration, and fusion. Fig. 7 summarizes this work flow. As we have only a single vision camera and do not use any other multiple or expensive sensors to capture scene data, we exploited our device's panning-tilting capability for stereo image acquisitions. We freely moved the imager in and around the environment from one place to another localizing gamma-rays passing through the detector and capturing corresponding scene images. Supposing the

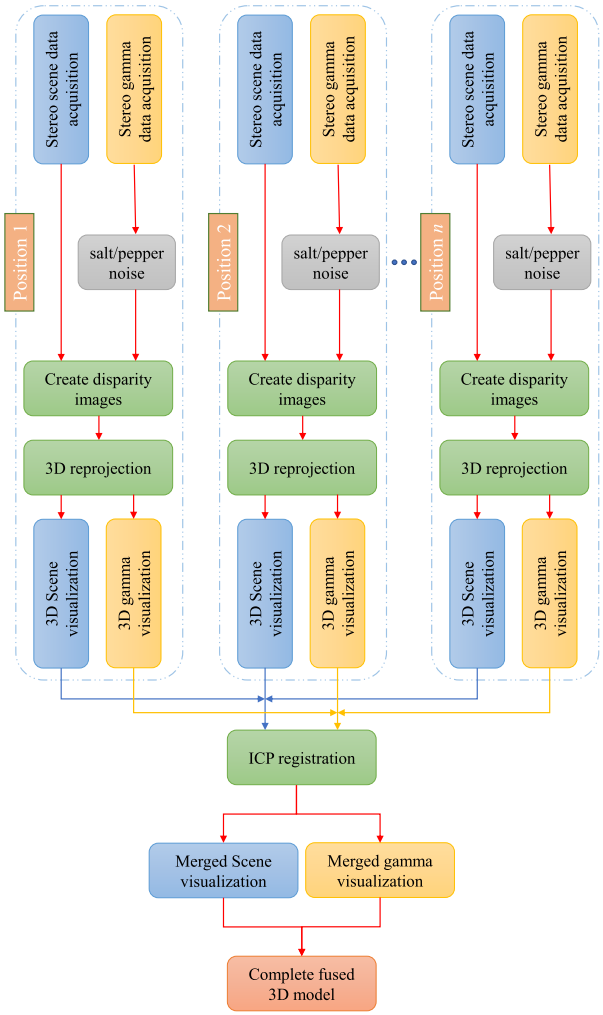

FIGURE 7. Flow of the proposed 3D visualizing method.

gamma detector lies on the left side and the vision camera on the right, we simultaneously capture a left gamma-ray image and a right scene image. Then we rotate the detector+camera unit by 180° vertically, and another 180° horizontally (interchanging two sensor positions with another) to capture the right gamma-ray image and the left scene image. After stereo images are acquired, we move the imager to another new location.

Stereo vision/matching has been one of the persistent ways of doing 3D reconstruction. The basis of general stereo vision denotes the problem of solving for dense correspondences between two viewpoints. Most of the previously introduced methods aim at finding-and-tracking, and mapping-and-localizing these correspondences - known as features in continuous image sequences to know the relative pose of the imager and to generate a 3D model of the surrounding environment. The reconstructions of gamma sources (most methods use the Maximum Likelihood Expectation Maximization - MLEM algorithm for gamma reconstructions [27]) are fused with these 3D models. However, we do not see the necessity of following the same 3D visualizing procedure

TABLE 1. Setting parameters for SGM algorithm.

Parameter name	Parameter value	
	Gamma	Vision
Census window	13	7
P1	15	9
P2	100	50
Aggregation paths	8	8
Minimum disparity	0	0
Maximum disparity	15	65
Image resolution	400×400	1280×960

when having access to gamma and scene stereo images. Instead of finding feature points and solving them using SLAM systems, we used reprojected depth data of disparity images to create detailed 3D reconstructions. We employed the well known SGM algorithm [19], [20], with Census cost function [32] to create disparity images of both the scene and the source.

SGM algorithm performs a pairwise matching to find best corresponding points between two images. In general, scene images have lot of distinguishable features, easing disparity estimation. But in contrast, gamma-ray images do not have rich features other than their mapped intensities (Fig. 6), leading into matching ambiguities. One solution is projecting a colored random 2D pattern from a projector, which however, is not very effective as gamma cameras fail to capture them. To remove mismatches from black background regions, we applied a random salt-and-pepper pattern on the visualized 2D images. This works as similar as projecting a physical 2D random pattern. We applied this pattern only on the background, masking-out the intensity regions. As the number of point correspondences in untextured regions increases, the quality of stereo matching also increases.

As for vision images, we projected the physical colored random pattern to increase the number of corresponding points and matching quality in low textured, repetitive and discontinuity areas. We create both left-disparity and right-disparity images and perform left-right consistency check (LR check) to densely remove mismatching and occlusions. We also apply the well known weighted median filter (WMF) [33], [34] to further remove erroneous matches/outliers from these ill-posed regions while preserving edges in disparity results. Fig. 8(a) and 8(c) show disparity images of a single-point Cs-137 gamma source (raw disparity without LR check or filtering) and its surrounding environment after LR check and WMF. Table 1 summarizes the setting parameters for SGM for both gamma and vision images that we have used in our experiments.

The relationship between 2D disparity d and 3D depth Z can be shown as in (5):

$$d = bf/Z, \tag{5}$$

where b and f represent the baseline and the focal length, respectively. Once we know internal camera parameters,

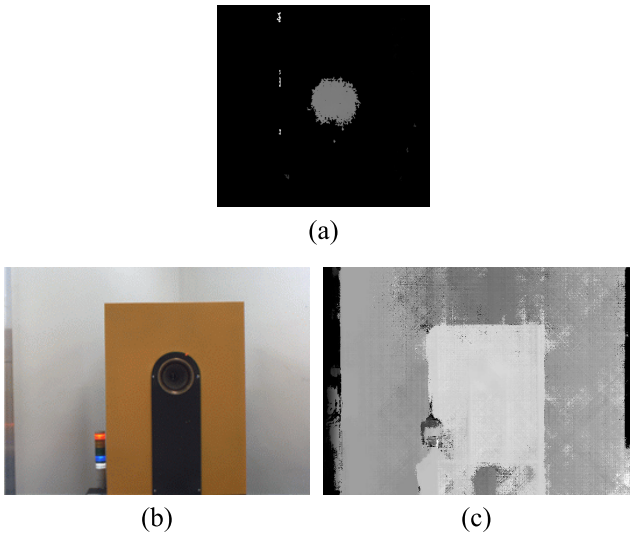

FIGURE 8. Disparity results of a Cs-137 point source: (a) gamma source raw disparity result without LR check or WMF, (b) left scene image, (c) scene disparity result with respect to left scene image after LR check and WMF.

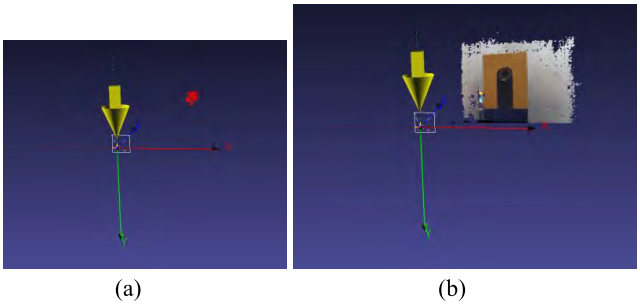

FIGURE 9. Reconstruction results by reprojecting disparities into 3D space: (a) gamma source reconstruction result, (b) scene reconstruction result. The yellow arrow shows the camera location with X, Y, Z axes.

we can easily project disparities into the 3D space to create a point cloud having X, Y, Z values for each pixel location. Fig. 9(a) and 9(b) show reconstruction results of above disparity images.

We repeated the same procedure at multiple locations while moving the imager from one place to another. We used the point-to-point ICP algorithm [21], [22] to merge and aggregate individual point clouds of scene contexts and gamma-ray sources separately. An identity matrix is used to represent the initial transformation relationship between two merges. Finally, these two aggregated point clouds are fused together to create a more detailed 3D model.

VI. EXPERIMENT RESULTS

In this section, results of distance measurements to gamma-ray sources and reconstructions employing our proposed 3D scene data fusion are presented. We performed our experiments using Cs-137 single-point gamma-ray source in a disclosed gamma facility, and LED light sources inside our laboratory. All the experiments are performed offline using a general purpose 64 bit windows10 desktop with an Intel(R)

FIGURE 10. Configuration setup for distance calculation.

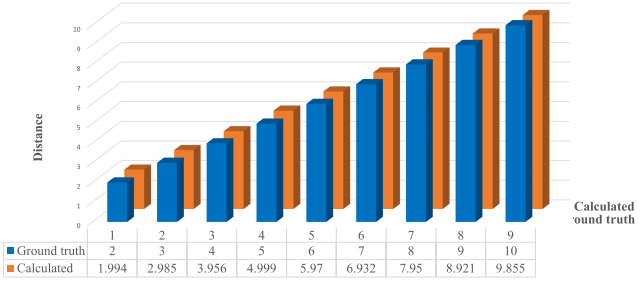

FIGURE 11. Comparing calculated distances with ground truth readings of a Bosch laser range finder.

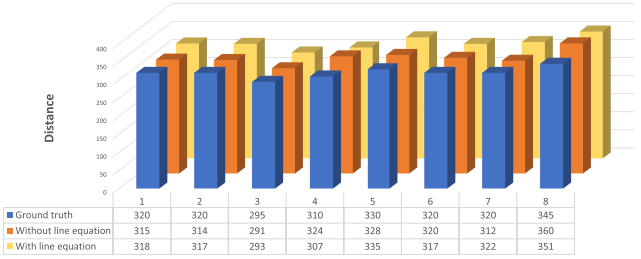

FIGURE 12. Qualitative distance analysis of 8-LED configuration. Calculated distances with and without applying proposed line equation model are compared with each other and ground truth values.

FIGURE 13. A forward representation of the Cs-137 source: (a) source is completely covered by a thick cardboard box, making it difficult to identify by the camera image, (b) an erroneous visualization of the source by overlaying isotopes above the scene image.

Core(TM) i7-7700 CPU at 3.60GHz, and 16GB RAM. We perform a quantitative analysis between calculated distances with respect to ground truth readings. Reconstruction and time complexity results of our method are qualitatively compared with the results obtained by the block matching algorithm [31] in OpenCV library [30].

A. 3D DISTANCE CALCULATION

We performed 3D distance estimation experiments as a mathematical way of identifying the existence and understanding the location of gamma-ray sources. In order to calculate 3D distances, we need to have stereo camera parameters of the gamma detector. Calibrating vision cameras is straightforward, where a series of calibration images are solved by the well known Zhang camera calibration method [29]. However, this method cannot be applied directly on gamma detectors as capturing calibration images is not possible. We have proposed a better stereo gamma detector calibration method in our previous research work [17].

Fig. 10 shows an instance of this distance calculation using a Cs-137 point source. The imager is kept at 2m away from the source, and moved it gradually to a maximum of 10m. The results are summarized in Fig. 11. We used a high accurate Bosch GLM-250 laser range finder to calculate the ground truth values. The calculated distances are compared quantitatively with respect to these ground truth readings. The total average error for all experiments was about 0.7048%. We are not going to discuss about distance calculation experiments in details; as this paper's main target is to exemplify 3D reconstruction and visualization of sources. More experiments and result discussions for distance calculation using different experiment setups are summarized in our previous research [17].

In among experiment setups, we use the eight-LED source configuration (Figure 11 in [17]) to simulate and check how well our proposed line equation model behaves in more complex scenarios. As summarized in our previous article, the average error before applying the proposed line equation for the P8E1 experiment was 2.09% (refer Table 5 in [17]). However, after applying, the average error reduced to 1.003(%). This quantitative analysis derives the accuracy of the line equation model even under difficult environment situations. These results are summarized in Fig. 12.

B. SCENE DATA RECONSTRUCTION

We performed two types of 3D visualizing experiments, one using the CS-137 gamma source, and the other using an LED. For simplicity, we captured stereo data at only three locations. To test the performance accuracy of our method, We covered the source completely from a thick cardboard box, making it invisible to our naked eye. If we follow the conventional way of overlapping 2D source distribution over vision images, Fig. 13 shows how overlapping of 2D distribution of the source with the scene looks like. This simple visualization is completely wrong as it induces that the source is distributed on above the cardboard.

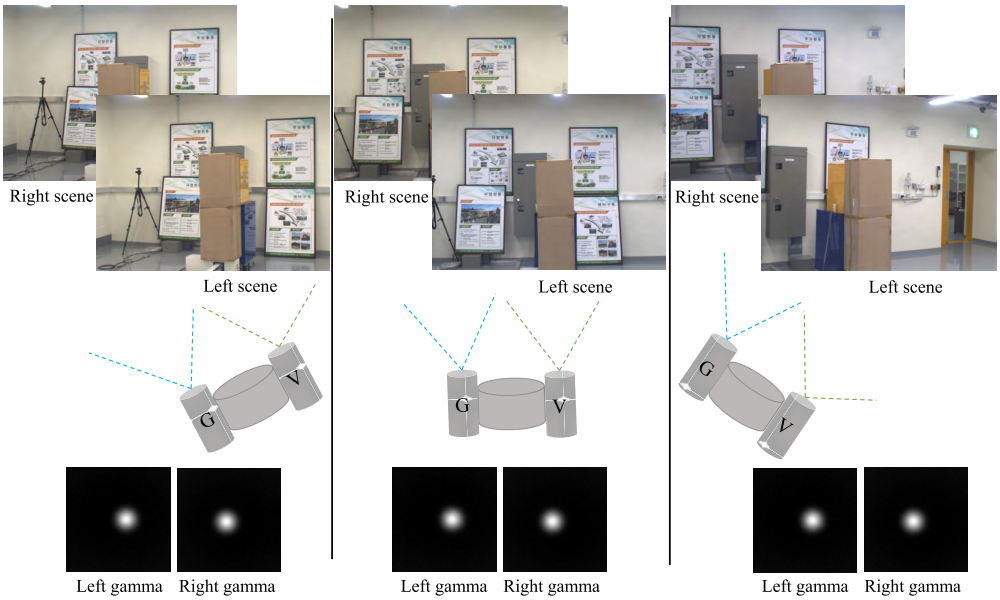

FIGURE 14. Stereo image acquisition by keeping the imager at three positions in the environment.

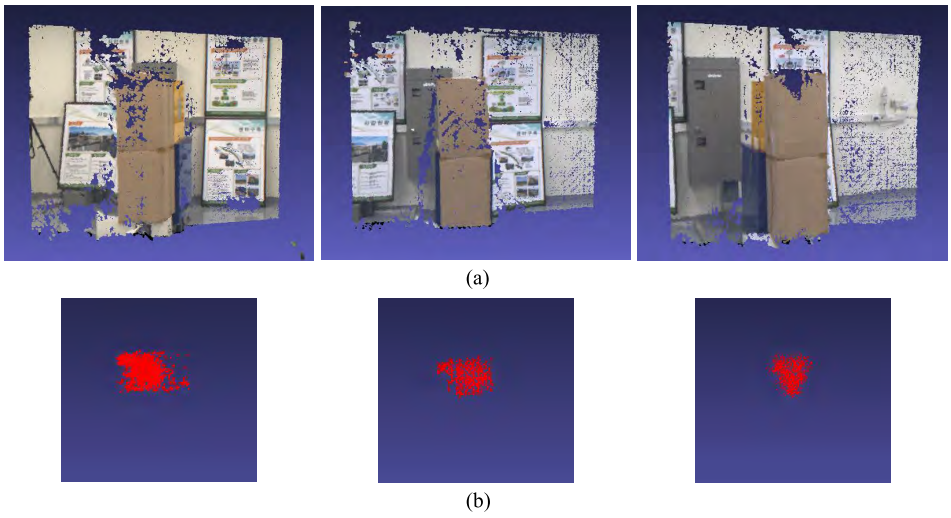

FIGURE 15. Reconstruction results of scene and gamma-ray images after reprojecting disparity images created with respect to left image.

To employ our proposed visualizing method, we captured stereo images at three positions by moving the imager freely, starting from right to left. Stereo scene and gamma-ray images are shown in Fig. 14 and their respective reconstructions are in Fig. 15. As shown in Fig. 15(a) we deliberately cropped a few 3D points at the left side of left and middle reconstructions. This is done purposefully to remove a few number of flying points that affected the reconstruction quality. Individual scene and gamma-ray reconstructions are merged with each other separately based on point-to-point ICP and fused together to create a complete and detailed 3D model. A front and top view of this complete 3D model is shown in Fig. 16. The results of the experiment we performed using the LED source are summarized in Fig. 17. In addition, a qualitative reconstruction comparison of the results obtained by our proposed reconstruction and block matching for the covered source is summarized in Fig. 18. Reconstruction result of block matching contains a few erroneous mismatches appeared due to incorrect matches between point correspondences. Comparing reconstruction results emphasizes the accuracy of our approach over the block matching algorithm.

The integration of point clouds using ICP consumes some time. The total execution time for disparity creation and scene fusion ranged from 5 minutes up to 10 minutes; depending on the complexity of the scene. As of this reason, currently,

FIGURE 16. A front and top view of the fused 3D model for Cs-137 source. The model solves the visual ambiguity of overlaying 2D isotopes above vision images. Gamma source shown in red color lies behind the obstacle.

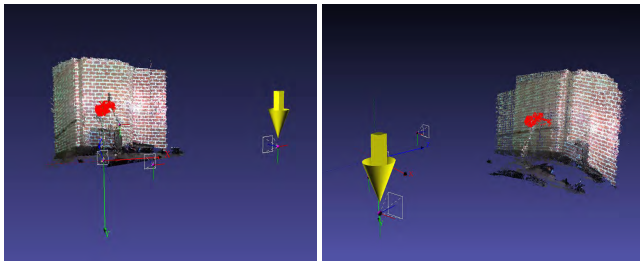

FIGURE 17. A front and side view of the fused 3D model for LED source. The model helps to distinguish the source location with its environment context.

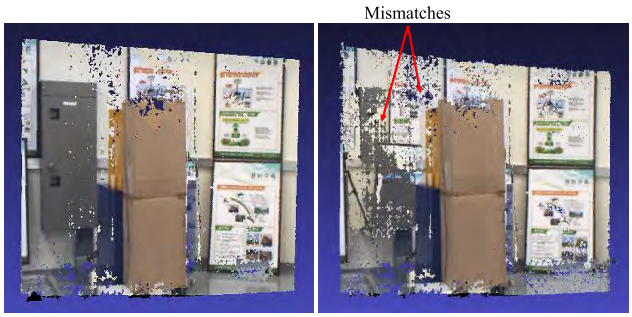

FIGURE 18. Qualitative comparison between two reconstruction results. left: SGM-based reconstruction, right: block matching-based reconstruction.

the proposed scene fusion is performed offline. The estimated time for SGM-based approach was about 8 minutes, where it was about 11 minutes for Block matching-based approach.

VII. CONCLUSION

Scene data fusion with gamma-ray source reconstructions provides unprecedented capabilities in identifying actual locations of sources that are relevant for the application in many radioactive researches. This paper demonstrated a modest scene data fusion technique using a pan/tilt type gamma-ray imaging system. Unlike most state-of-the-art imagers, we did not integrate multiple or high expensive contextual sensors such as, LiDAR or Kinects to reconstruct scene environment. We integrated only a single vision camera along with the gamma detector and captured stereo images by rotating the imager horizontally and vertically, while moving it in and around the environment. We proposed a noval line equation model to properly localize gamma sources passing through the opening of the collimator, while compensating misalignment problems of the gamma detector. Instead of using SLAM techniques as in most existing methods, we proposed a modest reconstruction approach by reprojecting disparity images created based on stereo matching technique in computer vision into 3D space. We employed the well-known SGM algorithm as our base to create dense disparity images for both the gamma source and its surrounding scene environment. We calculated depth values at each pixel location of disparity results to update a 3D point cloud. We moved the imager freely around the environment to capture data at multiple locations, and merged respective reconstructions with each other using point-to-point ICP algorithm. We finally fused separately merged reconstructions of the source and the scene together to visualize the complete source shape and its distribution in the environment. We demonstrated that this approach can be easily used to remove visualizing ambiguities when overlapping 2D isotopes on above scene data. Currently, the proposed methods are validated for gamma-ray sources with simple geometries, and both 2D visualizations and 3D reconstructions are performed offline. As future work, we are planning to extend our studies into sources that are widely distributed in the environment, while capturing data at more than three locations, and GPU parallelizing individual processes to achieve near real time running capabilities. Also, in addition, we are planning to improve reconstruction merging quality by employing color ICP, instead of using point-to-point ICP.

REFERENCES

[1] K. Vetter, "Multi-sensor radiation detection, imaging, and fusion," *Nucl. Instrum. Methods Phys. Res. A, Accel. Spectrom. Detect. Assoc. Equip.*, vol. 805, pp. 127–134, Jan. 2016.

[2] D. Hellfeld, P. Barton, D. Gunter, A. Haefner, L. Mihailescu, and K. Vetter, "Omnidirectional 3D gamma-ray imaging with a free-moving spherical active coded aperture," in *Proc. IEEE Nucl. Sci. Symp. Med. Imag. Conf. (NSS/MIC)*, Atlanta, GA, USA, Oct. 2017, pp. 1–3.

[3] R. Barnowski, A. Haefner, L. Mihailescu, and K. Vetter, "Scene data fusion: Real-time standoff volumetric gamma-ray imaging," *Nucl. Instrum. Methods Phys. Res. A, Accel. Spectrom. Detect. Assoc. Equip.*, vol. 800, pp. 65–69, Nov. 2015.

[4] T. Takahashi, S. Takeda, S. Watanabe, and H. Tajima, "Visualization of radioactive substances with a Si/CdTe Compton camera," in *Proc. IEEE Nucl. Sci. Symp. Med. Imaging Conf. Rec. (NSS/MIC)*, Anaheim, CA, USA, Oct./Nov. 2012, pp. 4199–4204.

[5] J. Kataoka, A. Kishimoto, T. Nishiyama, T. Fujita, K. Takeuchi, T. Kato, T. Nakamori, S. Ohsuka, S. Nakamura, M. Hirayanagi, S. Adachi, T. Uchiyama, and K. Yamamoto, "Handy Compton camera using 3D position-sensitive scintillators coupled with large-area monolithic MPPC arrays," *Nucl. Instrum. Methods Phys. Res. A, Accel. Spectrom. Detect. Assoc. Equip.*, vol. 732, pp. 403–407, Dec. 2013.

[6] D. Tomono, T. Tanimori, H. Kubo, A. Takada, T. Mizumoto, Y. Mizumura, T. Sawano, Y. Matsuoka, S. Komura, S. Nakamura, "First application to environmental gamma-ray imaging with an electron tracking compton camera," in *Proc. IEEE Nucl. Sci. Symp. Med. Imag. Conf.*, Seoul, South Korea, Oct./Nov. 2013, pp. 1–5.

[7] M. L. Giger, H. P. Chan, and J. Boone, "Anniversary paper: History and status of CAD and quantitative image analysis: The role of medical physics and AAPM," *Med. Phys.*, vol. 35, no. 12, pp. 5799–5820, Dec. 2008.

[8] L. Mihailescu, K. Vetter, W. Ruhter, D. Chivers, M. Dreicer, C. Coates, S. Smith, J. Hines, A. R. Caiado, V. Sequeira, M. Fiocco, and J. G. Goncalves, "Combined measurements with three-dimensional design information verification system and gamma ray imaging—A collaborative effort between oak ridge national laboratory, lawrence livermore national laboratory, and the joint research center at ISPRA," in *Proc. 47th Annu. INMM Meeting (INMM)*, Jul. 2006, pp. 16–20.

[9] K. Vetter, M. Burks, C. Cork, M. Cunningham, D. Chivers, E. Hull, T. Krings, H. Manini, L. Mihailescu, K. Nelson, D. Protic, J. Valentine, and D. Wright, "High-sensitivity Compton imaging with position-sensitive Si and Ge detectors," *Nucl. Instrum. Methods Phys. Res. A, Accel. Spectrom. Detect. Assoc. Equip.*, vol. 579, no. 1, pp. 363–366, Aug. 2007.
[10] K. Vetter, D. Chivers, and B. Quiter, "Advanced concepts in multi-dimensional radiation detection and imaging," in *Proc. Int. Symp. Radiation Detectors Their Uses (ISRD)*, 2015, pp. 179–192. doi: 10.7566/JPSCP.11.07000.
[11] L. Mihailescu, K. Vetter, and D. Chivers, "Standoff 3D gamma-ray imaging," *IEEE Trans. Nucl. Sci.*, vol. 56, no. 2, pp. 479–486, Apr. 2009.
[12] K. P. Ziock, "Principles and applications of gamma-ray imaging for arms control," *Nucl. Instrum. Methods Phys. Res. A, Accel. Spectrom. Detect. Assoc. Equip.*, vol. 878, pp. 191–199, Jan. 2018.
[13] M. J. Cieślak, K. A. A. Gamage and R. Glover, "Coded-aperture imaging systems: Past, present and future development—A review," *Radiat. Meas.*, vol. 92, pp. 59–71, Sep. 2016.
[14] K. Vetter, R. Barnowksi, A. Haefner, T. H. Y. Joshi, R. Pavlovsky, and B. J. Quiter, "Gamma-ray imaging for nuclear security and safety: Towards 3-D gamma-ray vision," *Nucl. Instrum. Methods Phys. Res. A, Accel. Spectrom. Detect. Assoc. Equip.*, vol. 878, pp. 159–168, Jan. 2018.
[15] A. Haefner, R. Barnowski, P. Luke, M. Amman, and K. Vetter, "Handheld real-time volumetric 3-D gamma-ray imaging," *Nucl. Instrum. Methods Phys. Res. A, Accel. Spectrom. Detect. Assoc. Equip.*, vol. 857, pp. 42–49, Jun. 2017.
[16] D. G. Lowe, "Distinctive image features from scale-invariant keypoints," *Int. J. Comput. Vis.*, vol. 60, no. 2, pp. 91–110, 2004.
[17] S.-H. Baek, P. Rathnayaka, and S.-Y. Park, "Calibration of a stereo radiation detection camera using planar homography," *J. Sensors*, vol. 2016, May 2015, Art. no. 8928096.
[18] M. J. Westoby, J. Brasingtonb, N. F. Glassera, M. J. Hambreya, and J. M. Reynoldsc, "'Structure-from-motion' photogrammetry: A low-cost, effective tool for geoscience applications," *Geomorphology*, vol. 179, pp. 300–314, Dec. 2012.
[19] H. Hirschmuller, "Stereo processing by semiglobal matching and mutual information," *IEEE Trans. Pattern Anal. Mach. Intell.*, vol. 30, no. 2, pp. 328–341, Feb. 2008.
[20] H. Hirschmüller, "Accurate and efficient stereo processing by semi-global matching and mutual information," in *Proc. IEEE Conf. Comput. Vis. Pattern Recognit.*, vol. 2. Jun. 2005, pp. 807–814.
[21] F. Pomerleau, F. Colas, and R. Siegwart, "A review of point cloud registration algorithms for mobile robotics," *Found. Trends Robot.*, vol. 4, no. 1, pp. 1–104, May 2015.
[22] F. Wang and Z. Zhao, "A survey of iterative closest point algorithm," in *Proc. Chin. Autom. Congr. (CAC)*, Jinan, China, Oct. 2017, pp. 4395–4399.
[23] I. Moreno and C.-C. Sun, "Modeling the radiation pattern of LEDs," *Opt. Express*, vol. 16, no. 3, pp. 1808–1819, Feb. 2008. [Online]. Available: http://www.opticsexpress.org/abstract.cfm?URI=oe-16-3-1808
[24] D. Singh, C. Basu, M. Meinhardt-Wollweber, and B. Roth, "LEDs for energy efficient greenhouse lighting," *Renew. Sustain. Energy Rev.*, vol. 49, pp. 139–147, Sep. 2015.
[25] T. N. Duong, T. Takamura, H. Watanabe, and M. Tanaka, "Light emitting diodes (LEDs) as a radiation source for micropropagation of strawberry," in *Transplant Production 21st Century*. Dordrecht, The Netherlands: Springer, 2000, pp. 114–118.
[26] P. Rathnayaka, S. H. Baek, and S. Y. Park, "Visualization and 3D distance measurement of gamma sources using enhanced bilinear interpolation," in *Proc. 22nd Korea-Jpn. Joint Workshop Frontiers Comput. Vis. (FCV)*, 2016, pp. 396–400.
[27] S. J. Wilderman, N. H. Clinthorne, J. A. Fessler, C.-H. Hua, and W. L. Rogers, "List mode EM reconstruction of Compton scatter camera images in 3-D," in *Proc. IEEE Nucl. Sci. Symp. Conf. Rec.*, vol. 2, no. 15, Oct. 2000, pp. 292–295.
[28] O. Rahnama, D. Frost, O. Miksik, and P. H. Torr, "Real-time dense stereo matching with ELAS on FPGA-accelerated embedded devices," *IEEE Robot. Autom. Lett.*, vol. 3, no. 3, pp. 2008–2015, Jul. 2018.
[29] Z. Zhang, "A flexible new technique for camera calibration," *IEEE Trans. Pattern Anal. Mach. Intell.*, vol. 22, no. 11, pp. 1330–1334, Nov. 2000.
[30] G. Bradski and A. Kaehler, *Learning OpenCV: Computer Vision With the OpenCV Library*. Sebastopol, CA, USA: O'Reilly Media, 2008.
[31] N. Einecke and J. Eggert, "Block-matching stereo with relaxed fronto-parallel assumption," in *Proc. IEEE Intell. Vehicles Symp.*, Jun. 2014, pp. 700–705.
[32] H. Hirschmuller and D. Scharstein, "Evaluation of cost functions for stereo matching," in *Proc. IEEE Conf. Comput. Vis. Pattern Recognit.*, Jun. 2007, pp. 1–8.
[33] Z. Ma, K. He, Y. Wei, J. Sun, and E. Wu, "Constant time weighted median filtering for stereo matching and beyond," in *Proc. IEEE Int. Conf. Comput. Vis.*, Dec. 2013, pp. 49–56.
[34] Y. Dong and S. Xu, "A new directional weighted median filter for removal of random-valued impulse noise," *IEEE Signal Process. Lett.*, vol. 14, no. 3, pp. 193–196, Mar. 2007.

PATHUM RATHNAYAKA received the B.Sc. and M.Sc. degrees in computer science and engineering from Kyungpook National University, Daegu, South Korea, in 2014 and 2016, respectively, where he is currently pursuing the Ph.D. degree with the School of Computer Science and Engineering. His research interests include stereo vision, stereo matching, and image processing.

SEUNG-HAE BAEK received the B.Sc. degree from the Department of Computer Engineering, Kyungpook National University, in 2004, and the M.Sc. and Ph.D. degrees in electrical engineering and computer science from Kyungpook National University, in 2010 and 2017, respectively. He is currently a Researcher with Orbotech, South Korea. His research interests include stereo matching, optics, and 3D reconstruction.

SOON-YONG PARK received the B.Sc. and M.Sc. degrees in electronics engineering from Kyungpook National University, Daegu, South Korea, in 1991 and 1999, respectively, and the Ph.D. degree in electrical and computer engineering from the State University of New York at Stony Brook, in 2003. From 1993 to 1999, he was a Senior Research Staff with KAERI, South Korea. From 2011 to 2018, he was a Professor with the School of Computer Science and Engineering, Kyungpook National University, where he is a Professor with the School of Electronics and Engineering. His research interests include 3D sensing and modeling, and multi-view 3D data processing.